Geomechanics and Engineering, *Vol. 24, No. 4 (2021) 389-397*
DOI: https://doi.org/10.12989/gae.2021.24.4.389

Effect of slope with overburden layer on the bearing behavior of large-diameter rock-socketed piles

Haofeng Xing*[1], Hao Zhang[1a], Liangliang Liu[1b] and Yong Luo[2c]

[1]Department of Geotechnical Engineering, Tongji University, Shanghai 200092, China
[2]Department of Geology Survey and Design,
Guizhou Transportation Planning Survey and Design Academe Co., Ltd., Guiyang, 550001, China

(Received January 12, 2020, Revised January 27, 2021, Accepted February 1, 2021)

Abstract. Pile foundation is a typical form of bridge foundation and viaduct, and large-diameter rock-socketed piles are typically adopted in bridges with long span or high piers. To investigate the effect of a mountain slope with a deep overburden layer on the bearing characteristics of large-diameter rock-socketed piles, four centrifuge model tests of single piles on different slopes (0°, 15°, 30° and 45°) were carried out to investigate the effect of slope on the bearing characteristics of piles. In addition, three pile group tests with different slope (0°, 30° and 45°) were also performed to explore the effect of slope on the bearing characteristics of the pile group. The results of the single pile tests indicate that the slope with a deep overburden layer not only accelerates the drag force of the pile with the increasing slope, but also causes the bending moment to move down owing to the increase in the unsymmetrical pressure around the pile. As the slope increases from 0° to 45°, the drag force of the pile is significantly enlarged and the axial force of the pile reduces to beyond 12%. The position of the maximum bending moment of the pile shifts downward, while the magnitude becomes larger. Meanwhile, the slope results in the reduction in the shaft resistance of the pile, and the maximum value at the front side of the pile is 3.98% less than at its rear side at a 45° slope. The load-sharing ratio of the tip resistance of the pile is increased from 5.49% to 12.02%. The results of the pile group tests show that the increase in the slope enhances the uneven distribution of the pile top reaction and yields a larger bending moment and different settlements on the pile cap, which might cause safety issues to bridge structures.

Keywords: rock-socketed pile; bearing behavior; centrifuge model test; slope degree

1. Introduction

To fulfill the requirements of geologic conditions at mountainous areas during the construction of rapid transit railways and expressways, piles are primarily used to brace the upper load of bridges or viaducts (Jeong *et al*. 2010, Seo *et al*. 2013, Liang *et al*. 2016, Yuan *et al*. 2017, Wang *et al*. 2018). Large-diameter rock-socketed piles of over 2.0 m in diameter are typically used in bridges with long span or high piers (Kou *et al*. 2016, Xu *et al*. 2017, Jafari *et al*. 2019). Owing to the action of unsymmetrical pressure around the pile, the slope with a deep overburden layer negatively affects the bearing capacity of the pile; however, this is still unclear.

Rock-socketed piles are critical in infrastructure projects and have been widely used in buildings, roads, bridges, airports, and terminals. To obtain the bearing behavior of such piles, many investigations have been performed using different methods, such as field tests (Sinnreich and Ayithi 2014, Xu *et al*. 2017, Xing *et al*. 2019), indoor model tests (Zhang and Wong 2007, Gao *et al*. 2011, Xing *et al*. 2014, Liu *et al*. 2018), numerical simulations (Kong *et al*. 2006, Armaghani *et al*. 2017, Zhang *et al*. 2019, Li *et al*. 2019), and theoretical analyses (Seola *et al*. 2008, Yu *et al*. 2013, Xing *et al*. 2017). These results from using these methods indicate that a rock-socketed pile does not belong to the entire end-bearing pile, and that the bearing capacity is influenced by many factors such as properties of the covering soil layer, rock strength, interface roughness of pile and rock, modulus ratio of pile and rock, degree of weathering of rock mass, length–diameter ratio of pile, and pile construction process. With the development of rapid transit railways and expressways at mountainous areas, rock-socketed piles are built on slopes to fulfill the requirement of geological conditions; therefore, some scholars have performed the research on the bearing characteristics of piles on hillsides (Mezazigh and Levacher 1998, Roh *et al*. 2019). The results show that the bearing mechanism and bearing capacity of piles on mountain slope are more complex than those of piles in flat ground owing to their unsymmetrical boundary conditions. Piles on a mountain slope not only bear the upper load, but also suffer from the drag force and shear force caused by the slope effect. These forces lower the bearing capacity of the pile and cause differential settlement of the pile group, thus

*Corresponding author, Associate Professor
E-mail: hfxing@tongji.edu.cn
[a]Ph.D. Student
E-mail: zhhao0106@163.com
[b]Ph.D. Student
E-mail: liuliangliang@tongji.edu.cn
[c]Ph.D.
E-mail: 2280130169@qq.com

ISSN: 2005-307X (Print), 2092-6219 (Online)

Fig. 1 Photograph of Tongzi River Bridge

adversely affecting the strength and stability of its superstructure (Dai *et al*. 2017, Armaghani *et al*. 2018, Chen *et al*. 2019, Zou *et al*. 2019).

The results above explain the bearing behavior and influencing factors of rock-socketed piles, but less results have been reported about the large-diameter piles on a mountain slope. Further, the bearing mechanism of rock-socketed piles on a mountain slope should be further explored. Owing to the topographic limitations and geologic conditions, it is extremely difficult to perform field loading tests of large-diameter rock-socketed piles in mountainous areas. To investigate the bearing characteristics of rock-socketed piles on hillsides and explore the effect of a slope with an overburden layer on a pile's mechanical mechanism, centrifuge model tests on single piles and a pile group were performed based on the Tongzi River Bridge project in the Guizhou province of China, and the test results were analyzed to obtain the bearing behavior and mechanical mechanism of large-diameter piles on a slope in this study.

2. Project overview

The Tongzi River Bridge is a primary component of the Chishui–Mogao Expressway project in Guizhou province, China, as shown in Fig. 1. The length of the bridge is 1131.6 m, and its maximum height is 222.6 m. The primary bridge pillar with a height of 175 m is supported by 20 piles of diameter 2.5 m and length 45 m, where the pile's rock-socketed length is 12.5 m and the size of the pier is 24 m (length) × 20.5 m (width) × 5 m (height), constructed with reinforced concrete.

The ground elevation of the bridge site is 400-630 m, and its geologic strata are primarily divided into an overburden layer and bedrock. The overburden layer with a thickness of 3.5 m to 35 m is composed of granular soil, gravel soil, and pebble soil; its cohesion force and internal friction angle are 10-15 kPa and 40-42°, respectively. At the site of the primary bridge pillar, the thickness of the overburden layer is approximately 27 m, and the underlying bedrock is moderately weathered gray limestone with the saturated uniaxial compressive strength of 30 MPa. Considering the size of the piles and the complex geological conditions, the centrifuge model tests were performed to explore the bearing characteristics of super-large-diameter rock-socketed piles on mountainous slopes and the effects of the slope on its pile group foundation.

Table 1 Similarity relationship for centrifuge model tests

Physical quantity	Symbol	Dimension	Prototype 1 g	Test model *n* g
Length	*l*	L	1	1/n
Displacement	*u*	L	1	1/n
Stress	σ	---	1	1
Strain	ε	---	1	1
Area	*A*	L^2	1	$1/n^2$
Quality	m	M	1	$1/n^3$
Density	ρ	ML^{-3}	1	1
Unit weight	γ	$ML^{-3}T^{-2}$	1	1
Force	F	MLT^{-2}	1	$1/n^2$
Moment	M	ML^2T^{-2}	1	$1/n^3$
Stiffness	EA	MLT^{-2}	1	$1/n^2$

3. Centrifuge model test

3.1 Test introduction

The beam centrifuge at the Tongji University of China with the maximum acceleration of 200g (g is the gravity acceleration) was used to perform the centrifuge model tests. The effective radius of gyration is 3.0 m, and the maximum payload is 750 kg. The maximum allowable continuous run time is 24 h. The model box size adopted in this experiment is 0.9 m (length) × 0.7 m (width) × 0.7 m (height). Based on the actual engineering conditions of the Tongzi River Bridge and the model box dimensions, a centrifugal acceleration of 100 g was used in this research. The similarity conditions listed in Table 1 were adopted to reflect the prototype's characteristics, and the centrifuge model tests were based on the theory of geotechnical centrifuge operation (Schofield 1980).

3.2 Test scheme

Based on the actual conditions of the Tongzi River

Table 2 Centrifuge model test program

Pile type	Test number	Slope / °	Pile diameter / cm	Pile length / cm	Rock-socketed length / cm
Single pile	1	0°	d=2.5	18d=45	5d=12.5
	2	15°			
	3	30°			
	4	45°			
Pile group	*a*	0°	d=2.5	18d=45	5d=12.5
	b	30°			
	c	45°			

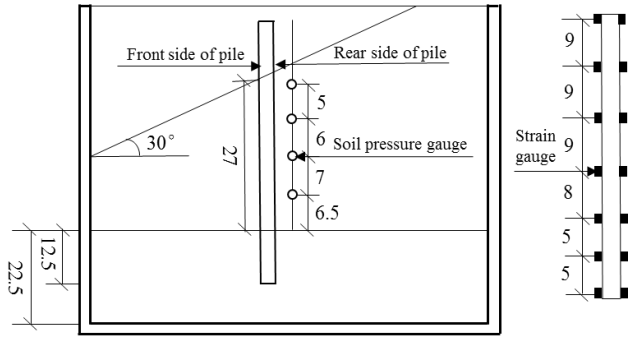

Fig. 2 Layout of single pile (unit: cm)

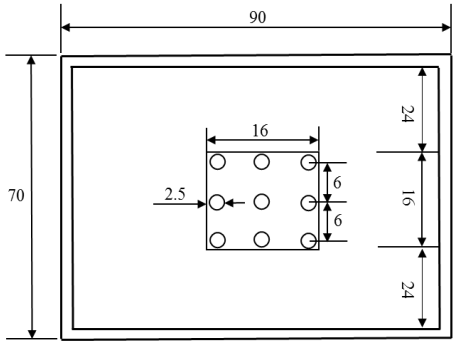

Fig. 3 Layout of pile group (unit: cm)

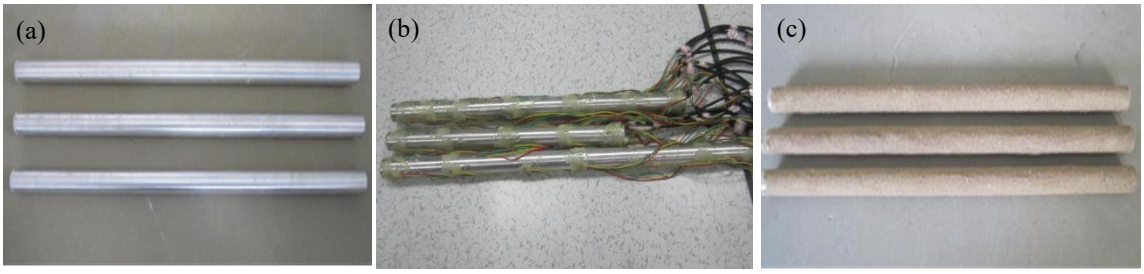

Fig. 4 Model piles made from aluminum alloy tube: (a) model piles, (b) Model piles with strain gauges and (c) Model piles with surface treatment

Bridge, four centrifuge model tests of single piles on different slopes varying from 0° to 45° were performed to investigate the effect of slope on the bearing characteristics of piles. In addition, three pile group tests were performed to explore the effect of slope on the bearing characteristics of the pile group. The slope varies from 0° to 45°, and the detailed test scheme is listed in Table 2. Because the overburden layers of a slope exceeding 45° are unstable, slopes exceeding 45° are not discussed herein. The rock-socketed length of the piles is 5d (d=pile diameter), as listed in Table 2. The layouts of the test models are shown in Fig. 2 and Fig. 3.

3.3 Production of model piles

According to the method described by Xing *et al*.

Table 3 Strength of soil sample for overburden layer

Test number	Normal pressure / kPa				c / kPa	φ / °
	50	100	150	200		
S1	52.0	92.5	141.1	174.5	11.0	41.2
S2	53.4	92.6	126.9	172.9	13.3	40.3
S3	47.9	105.3	139.6	177.3	11.9	40.2
S4	51.3	81.6	116.4	165.0	9.6	40.9
S5	48.9	100.1	129.4	176.1	10.9	40.8

Table 4 The uniaxial compressive strength of test block

No. of test block	1	2	3	4	5	6
Uniaxial compressive strength / MPa	29.58	29.07	28.54	29.50	29.51	28.96

Fig. 5 Single pile testing model at 45 degree slope

(2014), the large-diameter pile was simulated by seamless aluminum alloy tube, as shown in Fig. 4(a). The outer and inner diameters are 23 mm and 15 mm, respectively, and its elastic modulus is 70 GPa. Fourteen strain gauges were symmetrically plastered on the surface of the tube, as shown in Fig. 2 and Fig. 4(b), to protect the strain gauges and increase the model pile surface roughness, in which a 2-mm fiberglass cloth was used to cover it. The outer diameter of the tube was 25 mm after the model pile was completed, as shown in Fig. 4c. The strain gauge is small and flexible; the fiberglass cloth is flexible and is thinner than 0.2 mm. Sandblasting is performed to increase the model pile surface roughness and to hinder damages to the strain gauges during the installation of the model piles. However, because it was granular and non-continuous, even though it increased the diameter of the model pile, it is considered to influence the stiffness of the model pile only slightly.

The model pier was also made from aluminum alloy; its dimensions are 160 mm long, 160 mm wide, and 5 mm high, which meets the requirement of similarity.

3.4 Simulation of overburden layer

Based on the geological conditions of the Tongzi River Bridge, the overburden layer was simulated by a mixture of 30% clay and 70% quartz sand. To reach the state of saturation, water was added to the mixture. The mixture was fully stirred and subsequently consolidated under the pre-consolidation stress of 400 kPa, which is close to the effective pressure at the middle depth of the overburden layer. Five consolidated, quick, and direct shear tests were performed to test the strength index of this mixture, the results of which are listed in Table 3. The results show that the cohesion force and internal friction angle are close to the actual values. Therefore, the overburden layer can be simulated by this mixture.

Table 5 Increment of loading step

Loading step	Load of single pile / MN	Load of pile group / MN
1	20	100
2	31	200
3	42	300
4	51	500
5	61	---
6	71	---
7	82	---

3.5 Simulation of bedrock

Similar to the simulation of the overburden layer, the bedrock was simulated by a mixture of sand, cement, and water. A sand-cement-water-admixture ratio by mass of 300:1450:580:8 was adopted after many trials. After 28 days of normal curing, the axial compressive strengths of six mortar test blocks of size 70.7 mm × 70.7 mm × 70.7 mm were performed, and the results are listed in Table 4. The values of these tests range from 28.54 MPa to 29.58 MPa, with an average value of 29.19 MPa, which is close to 30 MPa. Therefore, the bedrock can be simulated by this mixture.

3.6 Centrifuge model instrumentations and process

In this test, a hydraulic pressure servo loading system and hydraulic jack with an accuracy of 1 N were adopted to apply the vertical load on the top of the single pile and the pile cap of the pile group. Geotechnical pressure sensors, ISE.CAEP, with a thickness of 2 mm, outer diameter of 8 mm, and measuring range of 1 MPa were used to measure the soil pressure. ACW-30 differential displacement sensors with a precision of 0.01 mm and a BX120-2AA resistance strain gauge with a sensitivity of 2.08 ± 1% were used to record the settlement of the pile top, and the pile strains were picked up by the strain gauge. Figure 5 shows the sketch of a single pile on a 45° slope. A step-loading technique was applied during the centrifuge model tests based on JGJ 106-2014, and the step-loading parameters are listed in Table 5.

4. Test results of single pile models

4.1 Pile's axial force

The pile is assumed to undergo elastic deformation under loading, and its axial force can be calculated from Eq. 1. Test number 3 (listed in Table 5) is used to indicate its axial force distribution characteristics.

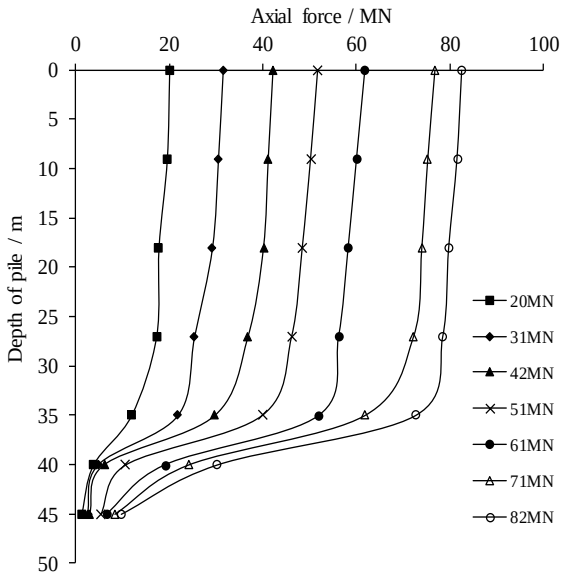

Fig. 6 Axial force distribution of pile with upper load change

Table 6 Load-sharing ratio of No.3 model pile

Vertical load / MN	Overburden layer		Bedrock layer		Tip resistance	
	Shared load / MN	Shared ratio / %	Shared load / MN	Shared ratio / %	Shared load / MN	Shared ratio / %
20	10.25	51.25	8.48	42.4	1.27	6.35
31	15.62	50.39	12.84	41.42	2.54	8.19
42	19.06	45.38	19.89	47.36	3.05	7.26
51	21.04	41.26	24.62	48.27	5.34	10.47
61	24.32	39.87	30.07	49.29	6.61	10.84
71	30.22	42.56	32.4	45.64	8.38	11.80
82	36.81	44.89	35.37	43.13	9.82	11.98

$$P = EA\left(\frac{\varepsilon_i + \varepsilon_j}{2}\right) \tag{1}$$

where E is the elastic modulus of the pile; ε_i and ε_j are the strains of the front and rear sides of the pile (as shown in Fig. 2), respectively; A is the cross-sectional area of the pile.

The axial forces shown in Fig. 6 indicate that the change trend of the pile's axial force along the pile length is similar under different loads. It reduces slowly in the overburden layer but decreases rapidly when the pile enters the bedrock layer. Table 6 lists the shared load and ratio of the overburden layer, bedrock layer, and pile end layer under each load, and it indicates that the overburden layer shares 39.87-51.25% of the total load. Its ratio decreases with the increase in the load and the bedrock layer constitutes approximately 40%. The load share ratio of the pile end layer increases with the increase in load, but it contributes only 6.35-11.98% and the trend gradually decelerates. Fig. 6 and Table 6 clarify that the bedrock layer presents a higher efficiency owing to its high strength. The overburden layer cannot be neglected when the bearing capacity of the pile is calculated, and the rock-socketed pile with an overburden layer belongs to the end bearing friction pile.

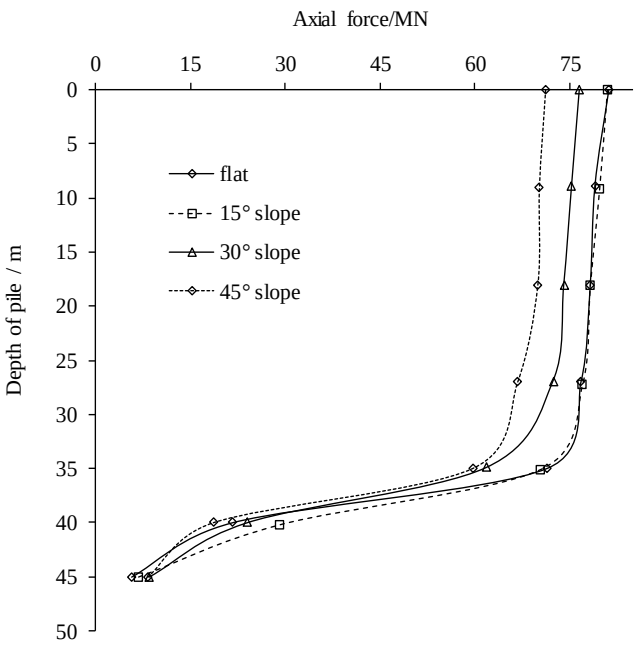

Fig. 7 Slope effect on pile's axial force

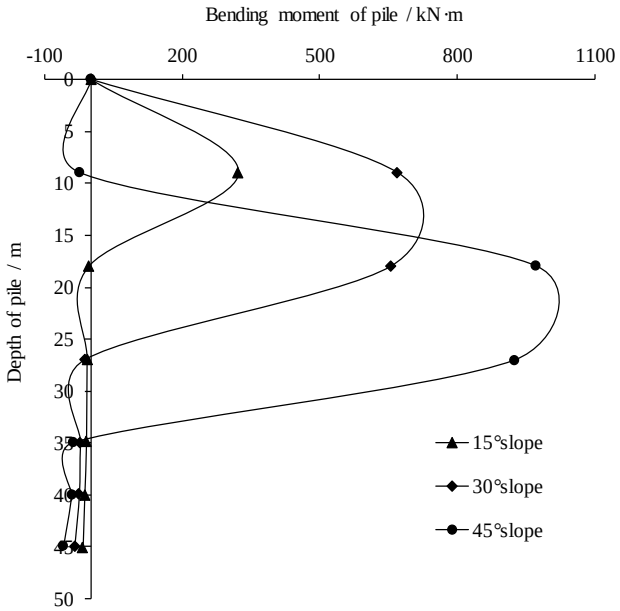

Fig. 8 Effect of slope variation on pile's bending moment

To explore the effect of the slope with an overburden layer on the pile's bearing capacity, the axial forces under the same settlement of 36 mm are compared as shown in Fig. 7. Owing to the effect of drag force caused by the asymmetric side slope, the pile's axial force caused by the upper load decreases when the slope increases from 0° to 45°, and the value lowers by more than 12% at 45° compared to that of the flat ground. Meanwhile, the pile's settlement under the same upper load also increases with the increase in the slope steepness. Using 82 MN as an example, the pile's settlements of 0, 15, 30, and 45 gradient slopes are 36.67 mm, 37.25 mm, 38.92 mm, and 40.01 mm, respectively.

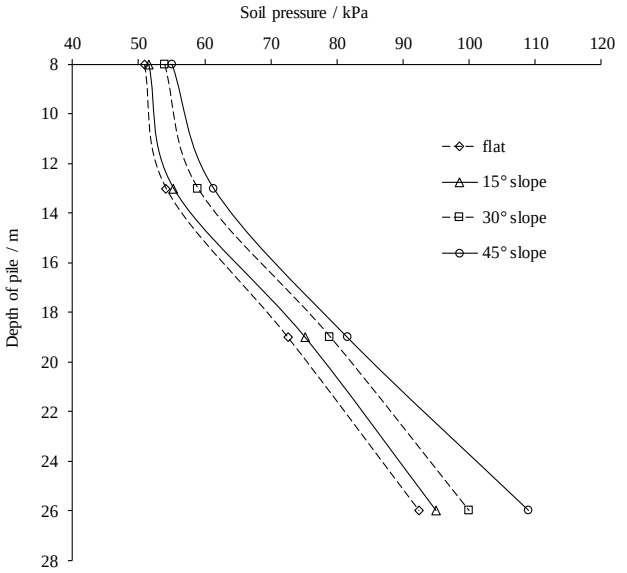

Fig. 9 Effect of slope variation on soil pressure

4.2 Bending moment of the pile

Shear and bending moment present adverse effects on the pile's stability; therefore, the bending moment caused by a slope with an overburden layer is investigated herein. Eq. (2) can be used to calculate the pile's bending moment.

$$M = \frac{EI\left(\varepsilon_i - \varepsilon_j\right)}{D} \tag{2}$$

where M is the pile's bending moment; E is the elastic modulus of the pile; I is the moment of inertia of the cross section; ε_i and ε_j are the strains of front and rear side of pile, respectively; D is the external diameter of the pile.

To obtain the effect of a slope with an overburden layer on a pile's bending moment, the calculated results of a pile's bending moments under 82 MN upper load are compared, as shown in Fig. 8. It is obvious that the variation in slope not only affects the value of the bending moment, but also changes its distribution. The piles of 15° and 30° exhibit similar change trends in bending moment, i.e., increasing with depth to the maximum value and subsequently rapidly decreasing to reverse the bending moment. However, the maximum bending moment at 30° is more than twice than that at 15°. Nevertheless, the bending moment of the pile at 45° exhibits a different change trend. Reverse bending moment occurs initially; subsequently, positive bending moment increases with depth to the maximum value and decreases rapidly similar to the pile at 30°. Its maximum bending moment (1085 kN·m) is more than three times that of (322 kN·m) the 15° case. Figure 8 also shows that the bending moments are primarily distributed in the upper part of the pile, and has wider distribution area with the increase in the slope steepness. Therefore, the effect of the slope on the pile should be considered when the designing large-diameter piles to be placed on hillsides.

4.3 Soil pressure and shaft resistance

To explore the relationship between the shaft resistance of the pile and its surrounding soil, four soil pressure gauges are evenly distributed at the rear side of the pile with a double pile diameter distance as shown in Fig. 2. The soil pressure under a vertical load of 82 MN is used to state the effect of slope on soil pressure, as shown in Fig. 9. When the depth is less than 12.5 m, the soil pressure shows a slow nonlinear increase with depth and its change trend at four different slope conditions is similar. However, when the depth exceeds 12.5 m, the soil pressure shows a rapid linear increase with the increase in slope steepness, and a higher increasing rate is shown at the 45° slope. Therefore, the slope changes the soil pressure and affects its distribution characteristics as well.

Owing to the slope, the soil in both the front and rear sides of the pile is unequal, thus leading to the asymmetry of stress at both sides of the pile. With the increase in slope, the soil height difference increases, causing the asymmetry of stress to be more obvious. As is known, the shaft resistance of the pile is significantly related to its surrounding pressure; therefore, the soil pressure difference at both sides of the pile will cause the corresponding difference of the pile's shaft resistance. The pile's shaft resistance is calculated through Eq. (3) and its difference at the front and rear sides of the pile can be acquired using Eq. (4). The shaft resistance of single piles under a vertical load of 82 MN is compared herein, and the distribution of shaft resistance at the front side of the pile is shown in Fig. 10; their maximum shaft resistances are listed in Table 7.

$$P = EA\varepsilon \tag{3}$$

$$T = \frac{P_i - P_{i+1}}{\pi D h} \tag{4}$$

where P_i and P_{i+1} are the pile's vertical force at i depth and $i+1$ depth; T is the shaft resistance of the pile; E is the elastic modulus of the pile; is the pile's elastic strain; A is the cross-section area of the pile; D is the external diameter of the pile; h is the distance between the i and $i+1$ depths.

Fig. 10 shows that the slope variation does not transform the distribution trend of the pile's shaft resistance. In the overburden layer, the shaft resistance is low and presents a minor change; however, it sharply increases when the pile enters the bedrock, reaches the maximum at a depth of 37.5 m, and subsequently decreases at the same speed. Fig. 10 and Table 7 show that slope effect on shaft resistance is obvious; the increase in slope steepness not only lowers the value of shaft resistance, but also increases the difference in shaft resistance between the front and rear sides of the pile. Under an upper load of 82 MN, the maximum shaft resistance at the front side of the pile decreases from 1279.19 kPa to 1008.94 kPa with the slope increasing from 0° to 45°, i.e., a reduction of 21.13%. At the rear side, it decreases from 1279.19 kPa to 1049.14 kPa, i.e., a reduction of 17.98%. With the increase in slope, the difference in ratio between the front and rear sides of the pile is widened. For the 45° slope, the maximum shaft resistance at the front side of the pile is lowered by 3.98% compared to that of the rear side.

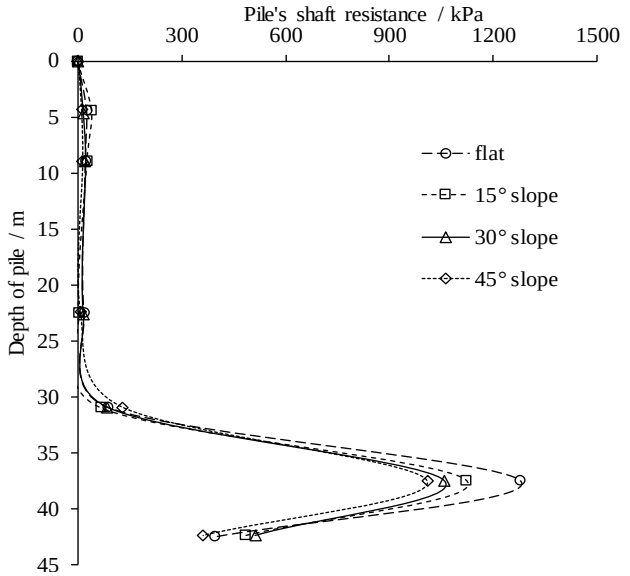

Fig. 10 Slope effect on the shaft resistance of pile's front side

Table 7 The effect of slope on the maximum shaft resistance of pile

Slope / °	Maximum shaft resistance at front side / kPa	Maximum shaft resistance at rear side / kPa	Difference ratio between rear and front sides / %
0	1279.19	1279.19	0
15	1122.25	1159.21	2.89
30	1056.82	1095.32	3.64
45	1008.94	1049.14	3.98

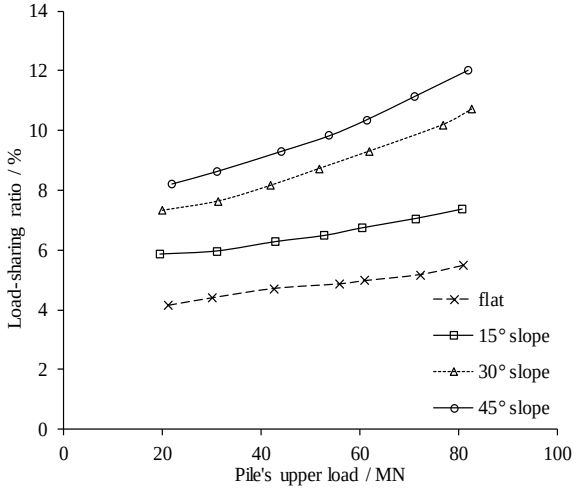

Fig. 11 Slope effect on load-sharing ratio of pile's tip resistance

4.4 Tip resistance of the pile

Similar to the effect of the slope on the lateral surfaces of the pile, the slope also affects the mechanical characteristics of the pile end. To understand its effect on the pile end, the load-sharing ratios of the pile's tip resistance to the upper load are acquired from the test results, as shown in Fig. 11. For the flap ground, the load-sharing ratio is gradually increased with the increase in the pile's upper load, increasing from 4.12% to 5.49 % when loaded from 20 MN to 82 MN, i.e., only a 1.36% increment. However, the slope gradient increase has increased the load-sharing ratio of the pile's tip resistance, accelerating with the increase in the pile's upper load. When loaded by 82 MN, the load-sharing ratios at slope degrees of 0, 15, 30, and 45 are 5.49%, 7.37%, 10.98%, and 12.02%, respectively. This means that the slope with an overburden layer causes an additional stress at the pile end, which will lower the strength of the pile's tip resistance.

The analyses above indicate that the slope adversely affects both the pile's shaft and tip resistances. Its drag load will yield additional shaft and tip resistances when the upper load is unchanged, and is accelerated with the increase in slope. Therefore, the slope reduces the pile's bearing capacity and its adverse effect expedites with slope gradient increase; this should be considered during pile design.

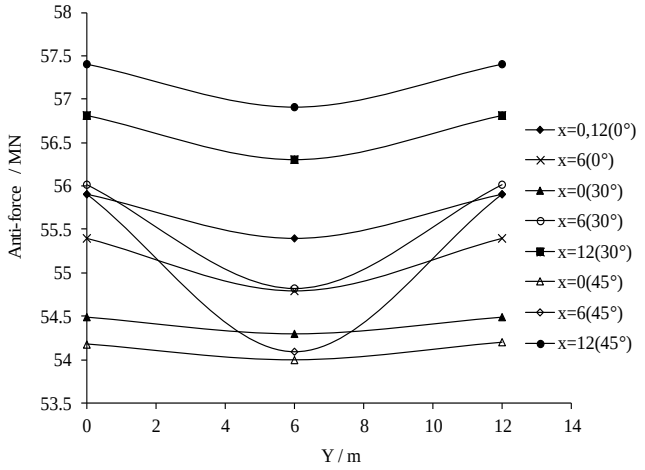

Fig. 12 Load distribution of piles under 500 MN applied load

Table 8 Sharing load of group piles under 500 MN load (MN)

Y/X	0° slope			30° slope			45° slope		
	0	6	12	0	6	12	0	6	12
0	55.91	55.39	55.91	54.49	56.01	56.81	54.18	55.91	57.40
6	55.39	56.79	55.39	54.29	56.81	56.31	53.99	58.09	56.90
12	55.91	55.39	55.91	54.49	56.01	56.81	54.18	55.91	57.40

4.5 Slope effects on pile-group behavior

To show the effect of a slope with an overburden layer on the pile group behaviour, a Cartesian coordinates system is established for the location of each pile in the group, as shown in Fig. 3. Three rows of piles along the x-direction and y-direction were spaced 6.0 m apart.

Similar to the single pile, the slope with an overburden layer has an apparent effect on the force and settlement of the pile group. The sharing load of the pile group is listed in Table 8 under the applied load of 500 MN, and the sharing

load of the piles in the Y direction are shown in Fig. 12. In the Y direction, which is perpendicular to the slope, the reaction force of the pile tip is symmetrical owing to the symmetry of the Earth's confining pressure and its value increases slightly with the increase in the slope gradient. However, along the X direction, which is parallel to the slope, the distribution of the pile top reaction is uneven and becomes increasingly obvious as the slope increases. From Table 8, the maximum load differences on the pile top at the 30° and 45° slopes are 2.32 MN and 3.22 MN, respectively, which correspondingly yield eccentric bending moments of 39.96 MN·m and 56.1 MN·m, respectively, along the slope direction. Meanwhile, their settlement differences are 8.76 mm and 10.57 mm respectively under the applied load of 500 MN. This settlement difference will result in a significant superstructure tilt of the super-high pier. The results clearly indicate that slope not only affects the load distribution of the pile group, but yields significant bending moments and results in an obvious differential settlement. This is not beneficial to the safety of the superstructure and its regular service.

5. Conclusions

Centrifuge model tests were performed to study the effects of slope on the mechanical characteristics of large-diameter rock-socketed piles. The conclusions are as follows:

(1) Centrifuge model tests could be successfully used to explore the influence of slope with an overburden layer on the mechanical characteristics of large-diameter piles. Further, the similarity ratio for the preparation of piles, soil, and rocks could fulfill the requirement of equivalent physical and mechanical properties;

(2) Slopes with an overburden layer caused a drag force that increased the axial force of the pile and adversely affected the pile's bearing capacity and settlement. Further, it will gradually increase with the increase in slope steepness. For the same settlement of 36 mm, the axial force of large-diameter rock-socketed pile was reduced by more than 10% with the slope increase from 0° to 45°. The converse was shown, in that approximately 9% of additional pile settlement will be yielded under the same upper load of 82 MN;

(3) The stress asymmetry of a slope with an overburden layer changed the distribution of the pile's shaft resistance and caused the bending moment on large-diameter piles. The increase in the slope gradient reduced the shaft resistance of the pile and intensified the difference between the front and rear sides of the pile. The maximum bending moment of the large-diameter pile at the 45° slope was more than thrice that of the 15° slope, and the 45° slope lowers the maximum shaft resistance by 3.98% at the front side of pile instead of the rear side;

(4) The increase in slope accelerated the load-sharing ratio of the tip resistance of the pile to its upper load. Under an 82-MN load, the load-sharing ratios at 0, 15, 30, and 45° slopes were 5.49%, 7.37%, 10.98%, and 12.02%, respectively, where an increment of approximately 7% occurred with an increase in the slope from 0° to 45°;

(5) Similar to the single pile, the pile group was adversely affected by the slope with an overburden, as well. With the increase in slope, the distribution of the pile top reaction became more uneven, thus causing a larger bending moment and different settlements. Compared with the flap ground, a 56.1-MN·m eccentric bending moment and a 10.57-mm differential settlement emerged on the pile cap at the 45° covered slope under a 500-MN upper load, which was detrimental to superstructure safety and its regular service

Acknowledgments

The National Natural Science Foundation of China (Grant Nos. 41272292 and 41672273) funded this research project. This research was also substantially supported by the Guizhou Provincial Department of Transportation (Project No. 2010-122). The Key Laboratory of Geotechnical and Underground Engineering of the Ministry of Education (Tongji University) has also provided a significant amount of support towards this study.

References

Armaghani, D.J., Faradonbeh, R.S., Rezaei, H., Rashid, A.S.A. and Amnieh, H.B. (2018), "Settlement prediction of the rock-socketed piles through a new technique based on gene expression programming", *Neural Comput. Appl.*, **29**(11), 1115-1125. https://doi.org/10.1007/s00521-016-2618-8.

Armaghani, D.J., Shoes, R.S.N.S.B.R., Faizi, K. and Rashid, A.S.A. (2017), "Developing a hybrid PSO-ANN model for estimating the ultimate bearing capacity of rock-socketed piles", *Neural Comput. Appl.* **28**(2), 391-405. https://doi.org/10.1007/s00521-015-2072-z.

Chen, X.Y., Zhang, M.Y. and Bai, X.Y. (2019), "Axial resistance of bored piles socketed into soft rock", *KSCE J. Civ. Eng.*, **23**(1), 46-55. https://doi.org/10.1007/s12205-018-0942-5.

Gao, R., Zeng, Y.J. and Zhu, B. (2011), "Centrifuge model testing on super-long rock-socketed bored piles under vertical loading", *Geomech. Geoeng.*, **6**(1), 21-29. https://doi.org/10.1080/17486025.2010.521590.

Dai, G.L., Salgado, R., Gong, W.M. and Zhu, M.X. (2017), "The effect of sidewall roughness on the shaft resistance of rock-socketed piles", *Acta Geotech.* **12**(2), 429-440. https://doi.org/10.1007/s11440-016-0470-8.

Jafari, M., Gharsallaoui, H., Victor, K.H. and Holeyman, A. (2019), "End bearing response of open-ended pipe piles embedded in rock", *Int. J. Rock Mech. Min. Sci.*, **119**, 46-57. https://doi.org/10.1016/j.ijrmms.2019.04.008.

Jeong, S., Ahn, S. and Seol, H. (2010), "Shear load transfer characteristics of drilled shafts socketed in rocks", *Rock Mech. Rock Eng.*, **43**(1), 41-54. https://doi.org/10.1007/s00603-009-0026-4.

Kong, K.H., Kodikara, J. and Haque, A. (2006), "Numerical modelling of the side resistance development of piles in mudstone with direct use of sidewall roughness", *Int. J. Rock Mech. Min. Sci.*, **43**(6), 987-995.

Kou, H.L., Guo, W., Zhang, M.Y. and Xu, Y.Q. (2016), "Axial resistance of long rock-socketed bored piles in stratified soils", *Ocean Eng.*, **114**, 58-65. https://doi.org/10.1016/j.oceaneng.2016.01.013.

Liang, X., Cheng, Q.G., Wu, J.J. and Chen, J.M. (2016), "Model

test of the group piles foundation of a high-speed railway bridge in mined-out area", *Front Struct. Civ. Eng.*, **10**(4), 488-498. https://doi.org/10.1007/s11709-016-0338-x.

Li, X.Y., Bai, X.Y. and Zhang, M.Y. (2019), "Study on bearing capacity characteristics of rock socketed short pile in weathered rock site", *J. Eng. Res.*, **7**(3), 76-89.

Liu, H.F., Zhu, C.Q., Meng, Q.S., Wang, X., Li, X.G. and Wu, W.J. (2018), "Model test on rock-socketed pile in reef limestone", *Rock Soil Mech.*, **39**(5), 1581-1588.

Mezazigh, S. and Levacher, D. (1998), "Laterally loaded piles in sand: Slope effect on P-Y reaction curves", *Can. Geotech. J.*, **35**(3), 433-441. https://doi.org/10.1139/t98-016.

Roh, Y., Kim, G., Kim, I. and Lee, J. (2019), "Effects of rock-support and inclined-layer conditions on load carrying behavior of piled rafts", *Geomech. Eng.*, **18**(4), 363-371. https://doi.org/10.12989/gae.2019.18.4.363.

Schofield, A.N. (1980), "Cambridge geotechnical centrifuge operation", *Geotechnique*, **30**(3), 227-268. https://doi.org/10.1680/geot.1980.30.3.227.

Seo, H., Prezzi, M. and Salgado, R. (2013), "Instrumented static load test on rock-socketed micropile", *J. Geotech. Geoenviron. Eng.*, **139**(12), 2037-2047. https://doi.org/10.1061/(ASCE)GT.1943-5606.0000946.

Seola, H., Jeong, S., Cho, C. and You, K. (2008), "Shear load transfer for rock-socketed drilled shafts based on borehole roughness and geological strength index (GSI)", *Int. J. Rock Mech. Min. Sci.*, **45**(6), 848-861. https://doi.org/10.1016/j.ijrmms.2007.09.008.

Sinnreich, J. and Ayithi, A. (2014), "Derivation of p–y curves from lateral pile load test instrument data", *Geotech. Test J.*, **37**(6), 20130127. https://doi.org/10.1520/GTJ20130127.

Wang, C.D., Zhou, S.H., Wang, B.L. and Guo, P.J. (2018), "Time effect of pile-soil-geogrid-cushion interaction of rigid pile composite foundations under high-speed railway embankments", *Geomech. Eng.*, **16**(6), 589-597. https://doi.org/10.12989/gae.2018.16.6.589.

Xing, H.F., Xiong, F., Wang, L.J. and Luo, Y. (2017), "Research on shaft resistance of rock-socketed piles based on the cavity expansion theory", *Mar. Georesour. Geotec.*, **35**(6), 873-877. https://doi.org/10.1080/1064119X.2016.1257670.

Xing, H.F., Zhang, Z., Meng, M.H. Luo, Y. and Ye, G.B. (2014), "Centrifuge tests of superlarge-diameter rock-socketed piles and their bearing characteristics", *J. Bridge. Eng.*, **19**(6), 04014010. https://doi.org/10.1061/(ASCE)BE.1943-5592.0000582.

Xing, H.F., Liu, L.L. and Luo, Y. (2019), "Effects of construction technology on bearing behaviors of rock-socketed bored piles as bridge foundations", *J. Bridge. Eng.*, **24**(4), 05019002. https://doi.org/10.1061/(ASCE)BE.1943-5592.0001368.

Xu, W., Liu, B., Zhou, Y.Q. and Han, Y.H. (2017), "Construction of 8.0-m diameter rock-socketed piles in a large-scale deep excavation", *Geotech. Geol. Eng.*, **35**(5), 2455-2466. https://doi.org/10.1007/s10706-017-0229-5.

Yuan, H.P., Zhao, P., Wang, Y.X., Zhou, H.L., Luo, Y. H. and Guo, P.P. (2017), "Mechanism of deformation compatibility and pile foundation optimum for long-span tower foundation in flood-plain deposit zone", *Int. J. Civ. Eng.*, **15**(6), 887-894. https://doi.org/10.1007/s40999-016-0066-6.

Yu, J., Cai, Y.Y. and Wu, W.B. (2013), "Effect of sediment on vertical dynamic impedance of rock-socketed pile with large diameter", *J. Cent. South Univ.*, **20**(10), 2856-2862. https://doi.org/10.1007/s11771-013-1806-2.

Zhang, L. M. and Wong, E.Y.W. (2007), "Centrifuge modeling of large-diameter bored pile groups with defects", *J. Geotech. Geoenviron. Eng.*, **133**(9), 1091-1101. https://doi.org/10.1061/(ASCE)1090-0241(2007)133:9(1091).

Zhang, X.L., Duan, B.C., Wang, C.Z. and Wang, D.Y. (2019), "Dynamic response analysis of lateral impact force of frame wharf with rock-socketed piles in Inland River steel sheath", *Adv. Civ. Eng.* 6918376. https://doi.org/10.1155/2019/6918376.

Zou, J.F., Yang, T. and Deng, D.P. (2019), "Field test of the long-term settlement for the post-grouted pile in the deep-thick soft soil", *Geomech. Eng.*, **19**(2), 115-126. https://doi.org/10.12989/gae.2019.19.2.115.

IC